Errors in finite element analysis of backward erosion piping

Robbins, B. A.; van Beek, V. M.; Pol, J. C.; Griffiths, D. V.

DOI
10.1016/j.gete.2022.100331

Publication date
2022

Document Version
Final published version

Published in
Geomechanics for Energy and the Environment

Geomechanics for Energy and the Environment 31 (2022) 100331

Contents lists available at ScienceDirect

Geomechanics for Energy and the Environment

journal homepage: www.elsevier.com/locate/gete

Errors in finite element analysis of backward erosion piping

B.A. Robbins [a,b,*], V.M. van Beek [c], J.C. Pol [d], D.V. Griffiths [b]

[a] U.S. Army Corps of Engineers, 12596 W Bayaud Ave Suite 400, Lakewood, CO, 80228, USA
[b] Department of Civil and Environmental Engineering, Colorado School of Mines, 1500 Illinois Street, Golden, CO, 80401, USA
[c] Unit Geo-Engineering, Deltares, Boussinesqweg 1, 2629 HV Delft, Netherlands
[d] Department of Hydraulic Engineering, Delft Univ. of Technology, Stevinweg 1, 2628 CN Delft, Netherlands

ARTICLE INFO

Article history:
Received 29 September 2021
Received in revised form 7 January 2022
Accepted 15 February 2022
Available online 21 February 2022

Editors-in-Chief:
Professor Lyesse Laloui and Professor Tomasz Hueckel

Keywords:
Backward erosion
Internal erosion
Finite element
Errors

ABSTRACT

Backward erosion piping (BEP) is a type of internal erosion responsible for the failure of many dams and levees. BEP occurs when small, shallow erosion channels progress upstream through foundation sands beneath the structure. As analysis of BEP involves coupling two different sets of flow equations to describe the groundwater flow and erosion pipe flow, the solution contains a singularity in the gradient field at the juncture of the soil and pipe domains. In addition, the erosion process is highly localized, often occurring over length scales of 1 cm or less. While it is well known that singularities and localized phenomena cause high errors in numerical solutions, there has been no assessment of the magnitude of these errors in BEP numerical models. This study evaluates the magnitude of error in BEP finite element models through comparison of numerical results to measurements from a highly instrumented BEP experiment. The results indicate that discretization errors related to the pipe geometry can cause 50%–300% error in the solution near the pipe tip when the pipe is represented via linear, 1D elements. These errors are significant and must be considered for models that assess pipe progression based on the local solution near the pipe tip. Results also indicate that the pipe width must be modeled as twice the physical pipe width to accurately represent the pipe flow when assuming a rectangular cross sectional shape for the erosion pipe.

Published by Elsevier Ltd.

1. Introduction

Backward erosion piping (BEP) is a type of internal erosion by which small, shallow erosion channels propagate upstream through foundation material along the contact of a pervious, sandy layer and a clay cover layer as illustrated in Fig. 1. The erosion progresses through the pervious sand layer as it is most erodible, and the presence of the clay cover layer is required for BEP to progress as it spans over the open pipe channels that form. If the erosion pipe connects to the upstream boundary, the flow will rapidly increase leading to pipe enlargement and collapse of the embankment. As numerous dam and levee failures have been attributed to BEP[1–3] the process is an issue of significant concern for engineers responsible for the safety of water resources infrastructure.

Over the past century, research has revealed many aspects of the erosion process (e.g., Refs. 5–18). In spite of the complexity of the BEP process, these studies have delivered a relatively complete description of the underlying physics driving BEP progression. With reference to the numbering in Fig. 1, the process of BEP involves (1) flow through porous media, (2) concentrated flow near a free exit to initiate erosion, (3) high seepage forces near the pipe tip due to concentrated flow, (4) mechanical failure (and detachment) of grains near the pipe tip, (5) laminar and turbulent flow of water through the erosion pipes that form, and (6) sediment pickup and transport of the eroded material along the full length of the erosion pipe. To accurately assess the potential for BEP to occur, an analysis must consider all subprocesses in a coupled manner.

While the various conditions that must occur for BEP to progress to failure are relatively well understood, there is currently no universally accepted method for analysis of BEP. The most commonly used approaches for assessing BEP are semi-empirical approaches that adjust critical values of average hydraulic gradients for BEP failure for contributing factors using a combination of empirical factors and groundwater flow theory[13,19]. While these methods have found widespread use, there remain many issues with the approaches that limit the accuracy for certain situations[4].

To eliminate the issues with semi-empirical approaches, there has recently been significant attention focused on the development of numerical tools to assess BEP progression (e.g., Refs. 12, 20–29). The primary appeal of more sophisticated numerical methods is the ability to readily perform site specific analysis

* Corresponding author at: U.S. Army Corps of Engineers, 12596 W Bayaud Ave Suite 400, Lakewood, CO, 80228, USA.
E-mail address: Bryant.a.robbins@usace.army.mil (B.A. Robbins).

https://doi.org/10.1016/j.gete.2022.100331
2352-3808/Published by Elsevier Ltd.

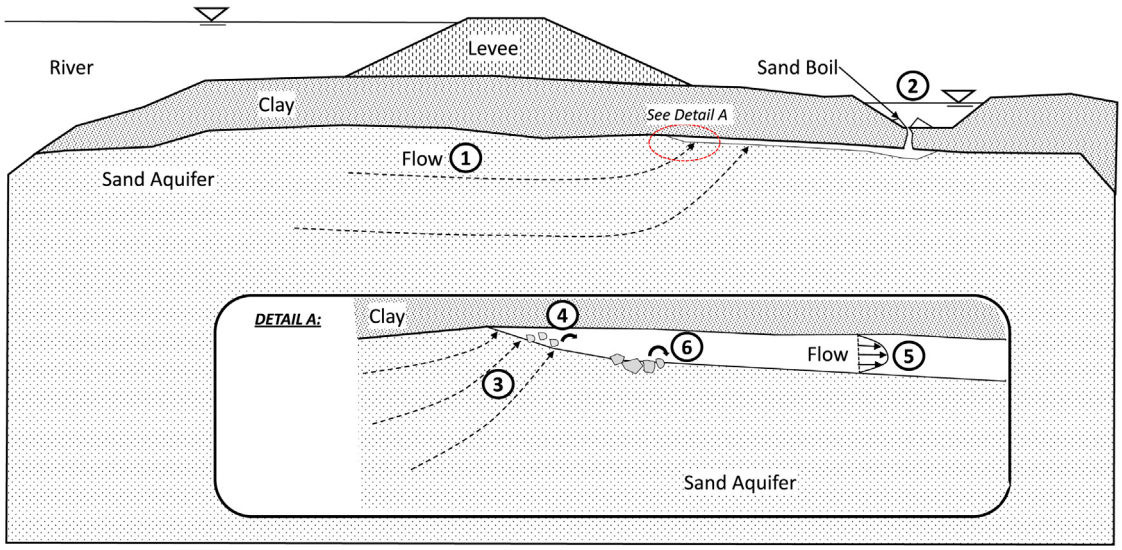

Fig. 1. Illustration of backward erosion piping beneath a levee[4].

that inherently includes all contributing factors simply based on the physics of the problem. The main challenge in developing numerical methods for BEP assessment is defining constitutive models and corresponding input parameters for the propagation of erosion. In the authors' opinions, no studies to date have presented a predictive method that has been robustly validated through numerical analysis of experiments and case histories using a rational means of selecting constitutive models and parameters a priori. All studies to date have presented numerical methods in the context of demonstrating a model and, in some cases, calibrating the model to a single data set. These would be considered C1 predictions according to Lambe[30] as the prediction is made after the event when the results are known. As noted by Lambe, C1 predictions are by far the most common in soil mechanics, however, one must be suspicious when an author uses C1 type predictions to 'prove' a technique is correct. To validate a method with C1 predictions, a systematic process must be employed that demonstrates reliable predictions of performance through numerous data sets and case histories. Early efforts to validate limit equilibrium slope stability methods followed this approach (e.g., Refs. 31, 32). Unfortunately, this has not yet been done for BEP models, largely due to the difficulty in defining erosion constitutive model parameters.

From the authors' experience, some of the difficulty in defining the erosion model input parameters may be caused by the model errors in the vicinity of the pipe tip. A singularity exists in the numerical solution at the tip of the erosion pipe due to the change in governing flow equations at this point. Additionally, the erosion process is a highly localized phenomena occurring over very small distances (order of a few grains of sand). It is well known that errors in numerical methods are significant for situations with singularities or highly localized phenomena. Despite this general knowledge, the magnitude of errors in BEP models has yet to be explored.

In the sections that follow, the errors in finite element (FE) analysis of BEP are explored through direct comparison to a highly instrumented BEP experiment. The FE model used for this study is first described, followed by a description of a single, highly instrumented laboratory test of BEP progression. FE analyses of the experiment are then presented to illustrate the influence of modeling assumptions (element size, pipe representation, etc.) on the numerical results. By comparing the model results to the experimental results, some inferences regarding the magnitude of errors in the FE solutions can be made.

2. Model description

A three-dimensional, piecewise, steady-state model[12] was used for simulating BEP in this study. While limited in capabilities compared to more sophisticated model formulations (e.g., Refs. 20, 25), a steady-state approach was well suited for this particular study because the laboratory experiment was allowed to reach an equilibrium state. Modeling an erosion pipe at equilibrium eliminated the temporal aspect of the process so that the study could focus solely on the quality of the hydraulic solution obtained from the finite element models. For general scenarios in practice, it may be necessary to use transient models to fully assess BEP risks.

The steady-state model used considers both the groundwater flow towards the pipe and the flow in the erosion pipes. The dimensions of the erosion pipes are determined based upon the sediment equilibrium conditions in the pipe, and the progression of the pipe is assessed based upon the hydraulic gradient just upstream of the erosion pipe. The erosion pipe can be represented using either hexahedral elements or 1D line elements. In the sections that follow, the governing equations, finite element formulation, and simulation algorithm for the FE model are described.

Governing Equations

The steady-state groundwater flow through the porous media towards the erosion pipe is described Eq. (1)

$$\frac{\partial}{\partial x}\left(k_x\frac{\partial h}{\partial x}\right)+\frac{\partial}{\partial y}\left(k_y\frac{\partial h}{\partial y}\right)+\frac{\partial}{\partial z}\left(k_z\frac{\partial h}{\partial z}\right)=0 \tag{1}$$

where $h = z+p/\gamma_w$ denotes the total head (potential) in terms of the elevation head z and the pressure head given in terms of the pore pressure p and the unit weight of water γ_w, and k_x, k_y, and k_z denote the hydraulic conductivity in the x, y, and z directions, respectively.

Under steady-state conditions for one dimensional pipe flow, the flow in the erosion pipes can be described by the Darcy–Weisbach equation

$$\frac{dh}{dx}=\frac{f}{D_H}\frac{V^2}{2g} \tag{2}$$

where f is the friction factor, $D_H = 4A/P$ is the hydraulic diameter of the pipe, A is the cross-sectional area of the pipe, P is the wetted perimeter of the pipe, V is the average velocity in the pipe, and g is the gravitational acceleration. In laboratory

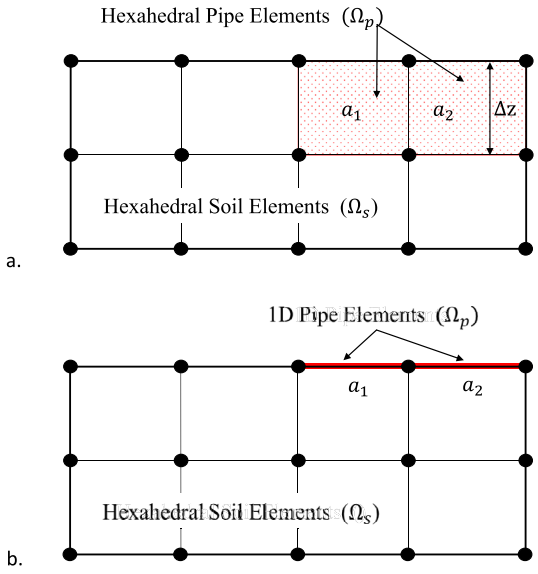

Fig. 2. Finite element discretization of BEP using (a) hexahedral pipe elements and (b) one-dimensional, rod pipe elements.

experiments, the pipes that form have been shown to have width to depth ratios of 10–50[16,17]. For cross sections of this shape, it is reasonable to approximate the pipe cross section as a rectangle of width w and depth a such that the hydraulic diameter is given by Eq. (3).

$$D_H = \frac{4wa}{2\,(w+a)} \tag{3}$$

Considering the case of $w \gg a$, D_H can be approximated by D_H^* which is only a function of the pipe depth.

$$D_H^* = 2a \tag{4}$$

The average pipe velocity in the pipe is given by

$$V = \frac{Q}{A} = \frac{Q}{wa} = \frac{q}{a} \tag{5}$$

where Q denotes the total flow rate in the pipe and q is the specific discharge (flow per unit width) in the pipe. Substituting Eqs. (4) and (5) into Eq. (2) yields the following governing equation for the pipe flow

$$\frac{dh}{dx} = \frac{fq^2}{4a^3g} \tag{6}$$

Assuming laminar flow conditions with the assumption that $w \gg a$, the friction factor is given by

$$f = \frac{48\mu}{\rho q} \tag{7}$$

where μ denotes the dynamic fluid viscosity and ρ is the fluid density. Substituting Eq. (7) into Eq. (6) and rearranging, the pipe flow equation takes the form of Darcy's equation

$$q = \frac{a^3\rho g}{12\mu}\frac{dh}{dx} = k_{pl}\frac{dh}{dx} \tag{8}$$

where k_{pl} is the equivalent hydraulic conductivity for laminar pipe flow in a pipe of depth a. It is convenient that the flow in the pipe takes this form as it permits the pipe flow equations to be integrated into the FE solution to Eq. (1). This will be demonstrated in the sections that follow.

The depth of the erosion pipes that form is dictated by the critical shear stress, τ_c, of the sand being eroded and transported[8,16], and the critical shear stress can be determined using the Shields' diagram or direct measurements[15]. The boundary shear stress, τ, on the bottom of the erosion pipe can be calculated as

$$\tau = \frac{a}{2}\rho g\frac{dh}{dx} \tag{9}$$

The depth of the erosion pipe will increase until $\tau < \tau_c$ and the sand grains on the bottom of the erosion pipe are at equilibrium.

The coupled solution to Eqs. (1), (8), and (9) solves the coupled groundwater flow, pipe flow, and sediment equilibrium equations for a given pipe position. To determine if the pipe will progress further, an additional criterion is required. For the present model, it has been assumed that the pipe progresses if a critical value of the horizontal, hydraulic gradient, i_c, is exceeded in the element upstream of the erosion pipe. That is, the pipe will progress further upstream if Eq. (10) is satisfied.

$$\sqrt{\frac{\partial h}{\partial x}^2 + \frac{\partial h}{\partial y}^2} > i_c \tag{10}$$

While Eq. (10) provides a means to assess if a pipe will progress, modeling the progression of the pipe is not necessary as part of this study. In this study, the model is used to compare the head profile calculated by the model to the head profile in an experiment with the pipe at equilibrium. As such, only the pipe dimensions (based on the sediment equilibrium) and pipe hydraulic conductivity need to be determined.

Finite element formulation

A cross section view through two finite element meshes, one using hexahedral pipe elements and one using 1D line pipe elements, is illustrated in Fig. 2. The problem domain consists of a soil domain, Ω_s, consisting of hexahedral soil elements and a pipe domain, Ω_p consisting of either hexahedral or 1D line pipe elements. Because the steady-state, laminar flow through the pipe elements takes the form of Darcy's equation (Eq. (8)), the coupled solution for the groundwater flow and pipe flow can be determined using a standard, steady-state groundwater flow solution. This analog has been used by many authors for simulating the BEP process (e.g., Refs. 12, 26, 27, 33). The finite element program for steady-state groundwater flow from Smith and Griffiths[34] was modified for this purpose. The finite element solution to Eqs. (1) and (8) is

$$[K_e]\{H\} = \{Q\} \tag{11}$$

where $\{H\}$ and $\{Q\}$ are vectors of the total head and net flow at the FEM nodes, and $[K_e]$ is the assembly of element conductivity matrices given by

$$[K_e] = \int_{\Omega_s}\left(k_x\frac{\partial N_i}{\partial x}\frac{\partial N_j}{\partial x} + k_y\frac{\partial N_i}{\partial y}\frac{\partial N_j}{\partial y} + k_z\frac{\partial N_i}{\partial z}\frac{\partial N_j}{\partial z}\right)d\Omega + \int_{\Omega_s} k_{pL}\left(\frac{\partial N_i}{\partial x}\frac{\partial N_j}{\partial x} + \frac{\partial N_i}{\partial y}\frac{\partial N_j}{\partial y} + \frac{\partial N_i}{\partial z}\frac{\partial N_j}{\partial z}\right)d\Omega \tag{12}$$

where N_i are the element shape functions and k_{pL} is the equivalent pipe hydraulic conductivity for the pipe. The value of k_{pL} can be inferred from Eq. (8) with adjustments made for the area of flow being represented. When using hexahedral pipe elements, the pipe width is represented by the element width. However, the element height is significantly larger than the actual pipe depth being represented. As such, the value of k_{pL} must be adjusted for the element height to represent the appropriate amount of pipe flow. For hexahedral pipe elements, k_{pL} is given by

$$k_{pL} = \frac{a^3\rho g}{12\mu\Delta z} \tag{13}$$

where Δz denotes the height of the hexahedral pipe element. For 1D, line pipe elements, the element has no physical dimensions

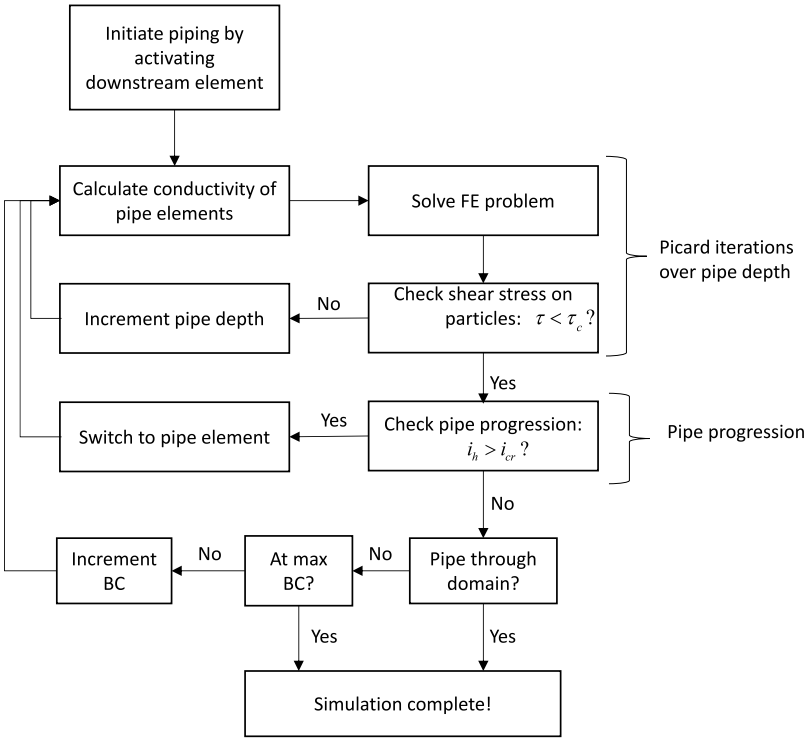

Fig. 3. Diagram of the simulation algorithm used for modeling pipe progression.

and the flow area must be accounted for entirely by the element conductivity. Maintaining the assumption of a rectangular pipe cross section with width, w, and depth, a, the equivalent hydraulic conductivity becomes

$$k_{pL} = \frac{a^3 \rho g}{12\mu} \cdot w \tag{14}$$

For a pipe depth of a given position and erosion pipe depth, the hydraulic solution is thus obtained by solving Eq. (11) over the domain with the appropriate value of k_{pL} used for the pipe elements based on the element type used to represent the erosion pipe.

Simulation algorithm

The previous section described the finite element formulation used to solve the coupled groundwater – pipe flow problem for a pipe of known position and depth. However, the depth of the pipe is not known *a priori* and must be determined as part of the solution. For the present study, the location of the pipe is known from observations during the laboratory experiment. However, this is typically not the case, and the position of the erosion pipe for a given set of boundary conditions must also be determined through an incremental, iterative procedure. The following paragraphs describe the simulation algorithm used for the generic case where both the pipe position and pipe dimensions are not known.

A diagram of the simulation algorithm is illustrated in Fig. 3. The erosion process is typically simulated by incrementally finding equilibrium states of the erosion pipe for gradually increasing boundary condition values. The boundary conditions are initially set to a nominal value with very little differential head. The erosion process is then simulated through the following steps:

1. Erosion is initiated by activating a pipe element at the desired initiation location. The depth of the pipe element is initialized to a value of $1 \times d_{50}$ based on observations in the laboratory of initial pipe depths[17].
2. The equivalent hydraulic conductivity of the pipe element is then calculated using Eq. (13) or Eq. (14) (depending on element type).
3. The FE problem is solved to obtain an initial hydraulic solution.
4. Using the updated hydraulic solution, the depth of the pipe element is checked to determine if $\tau < \tau_c$ by applying Eq. (9) and comparing to the defined value of τ_c for the sand. If the critical shear stress is exceeded, the pipe depth is increased by $d_{50}/2$ and the problem is solved again. These iterations continue until the pipe depth is determined in all pipe elements, thereby yielding the solution to the BEP problem that satisfies the conditions of sediment equilibrium in the erosion pipes. For the present study, this is the only portion of the algorithm required as the pipe position is known. Usually, however, the pipe progression must be evaluated as well by the following steps.
5. Once a valid solution has been obtained through the Picard iterations over the pipe depth, the pipe progression is evaluated by evaluating Eq. (10) in all soil elements adjacent to the pipe elements. If Eq. (10) is satisfied, the pipe will progress further. When using solely hexahedral pipe elements, the soil elements that satisfy Eq. (10) are switched to pipe elements resulting in an updated pipe position.
6. The iterations over the pipe depth are then repeated to evaluate the solution for the new pipe position. This process is repeated until Eq. (10) is no longer met in any soil elements adjacent to the erosion pipe indicating the pipe has come to equilibrium under the applied boundary condition.
7. At this point, the upstream boundary condition is increased slightly in value, and the simulation process (steps 1–6) is repeated until the pipe progresses through the domain or reaches a target boundary condition value.

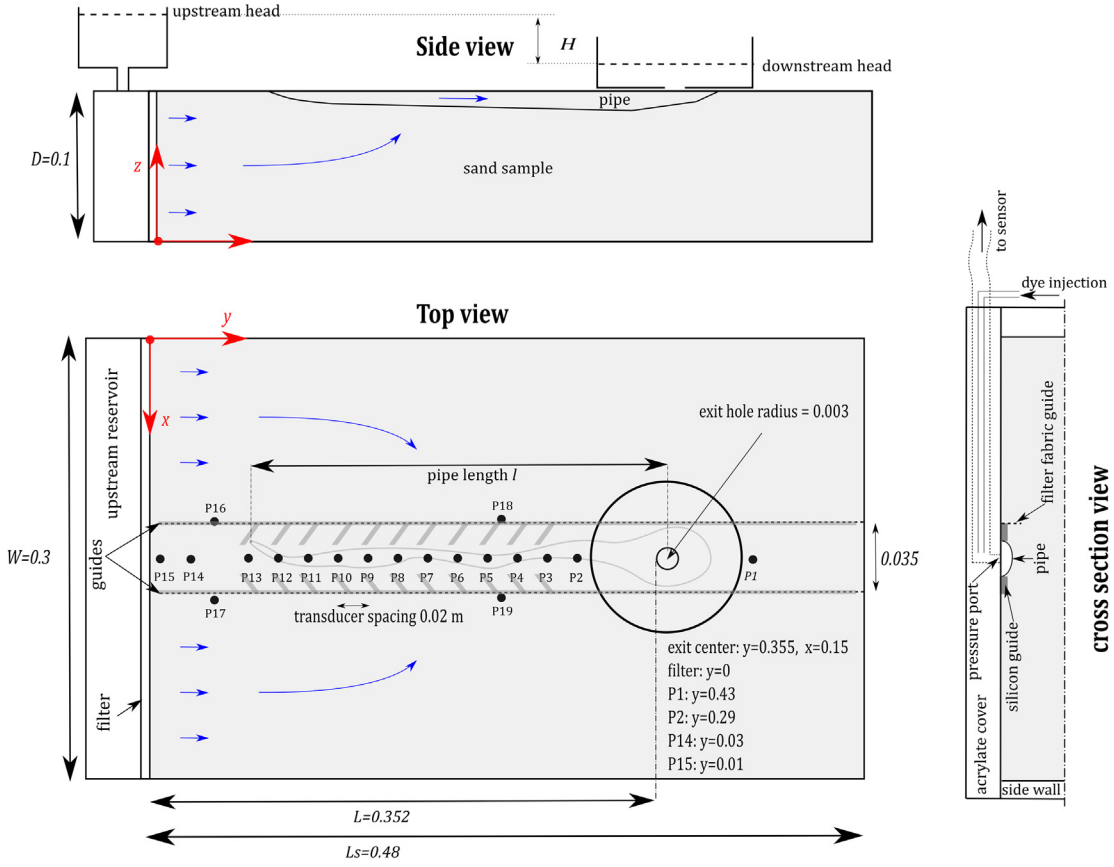

Fig. 4. Experimental setup[35].

When using 1D, line elements to represent the erosion pipe, the simulation algorithm follows exactly as previously described except that the soil elements are not switched to pipe elements. Instead, additional 1D line elements are activated and incorporated into the mesh in addition to the soil elements. The depth of the erosion pipe for the 1D line elements is evaluated the same way as before through Picard iterations over the pipe depth.

3. Piping experiment

A series of piping experiments were conducted in the Netherlands in rectangular samples with a restricted pipe path and dense array of pressure measurements. Because of the sample geometry and high sensor density, these tests provide a perfect data set for validation of BEP models. One test with test number B25-245 was particularly well suited for comparison purposes because (1) the pipe passed directly beneath the sensors and (2) the critical head was gradually approached such that the pipe stopped in equilibrium and the erosion channel cleared of sediment. This scenario matches the assumptions of the BEP model previously described and provides an excellent opportunity to validate numerical modeling procedures and evaluate the errors that exist in the solutions. A brief overview of this experiment is provided in the sections that follow. For further details, refer to Pol et al. 2022.

Description

The experiment consists of a rectangular soil sample that is 0.48 m in length, 0.30 m in width, and 0.10 m in depth as illustrated in Fig. 4. The sample has a constant head upstream boundary condition on the entire upstream wall of the box. The downstream outlet consists of a single hole through the acrylic top with a diameter of 6 mm. The differential head between the upstream and downstream water levels is incrementally increased to cause erosion to occur. For each head applied, the pipe is allowed to come to equilibrium at a given pipe length before the head is increased further. Once the critical differential head is reached, the pipe progresses the remainder of the way through the sample without stopping and the test is terminated.

As shown in Fig. 4, pore pressure measurements were made at 2 cm intervals along the pipe path to measure the head profile along the centerline of the sample. Pore pressures were measured by differential pressure transducers (Sensortechnics RPOP001D6 A) through the ports P1–P19 at a sampling frequency of 10 Hz. A photograph of the piping test is provided in Fig. 5.

The test reported here was conducted on Baskarp B25 sand, which has also been used previously by Akrami et al.[36] and Rosenbrand et al.[37]. The characteristics of the sand are given in Table 1. The minimum and maximum porosities were determined using the methods described in ASTM4253 (dry method, but vibrating needle instead of table) and ASTM4254 (funnel method).

The sample was prepared with the box in the vertical position with the upstream end of the box resting on a table. Dried sand was rained into de-aired water in the box and compacted by tapping the box with a hammer. Then the box is closed and placed in the horizontal position, and the head at both sides of the sample is leveled. The differential head was then gradually increased in intervals by lowering the downstream water level. The differential head was held constant at each interval until the pipe came to equilibrium and no further erosion was visible. Throughout the test, the pipe location was recorded with a camera, and the pressures were recorded.

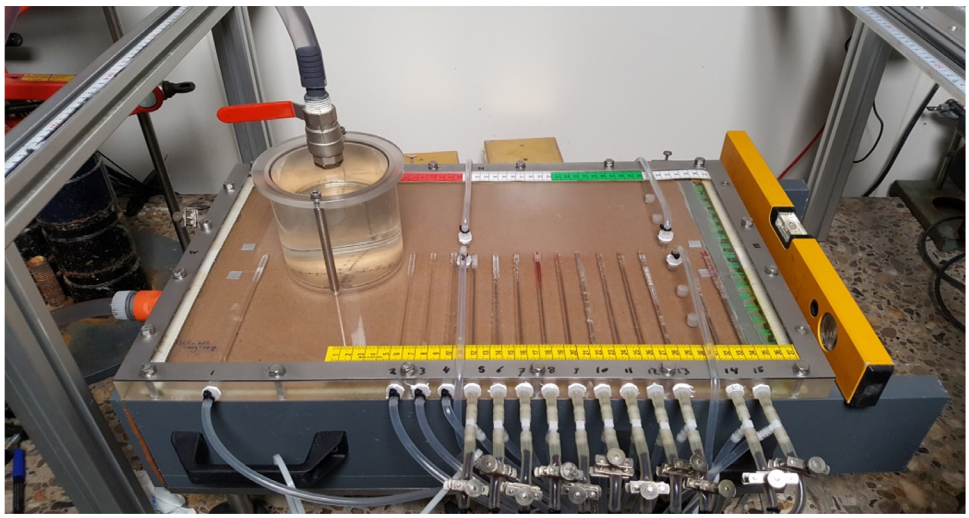

Fig. 5. Photograph of the experiment.

Table 1
Sand characteristics.

Sand type	d_{10} (mm)	d_{50} (mm)	d_{60} (mm)	d_{70} (mm)	C_u (-)	n_{min} (-)	n_{max} (-)	ρ_s (kg/m^3)
Baskarp B25	0.150	0.228	0.246	0.260	1.6	0.352	0.459	2650

Results

The erosion process observed can be broken down into three phases: fluidization at the exit, regressive erosion, and progressive erosion. These three phases are shown relative to the differential head applied to the sample and corresponding pipe position in Fig. 6. As the differential head was increased, the sand near the exit hole fluidized creating a small erosion cavity near the exit. This erosion cavity gradually enlarged until a distinct pipe began to form and progress in the upstream direction. The formation of a distinct pipe marked the beginning of the regressive erosion phase. During the regressive phase, the pipe would erode upstream with each increase in head and come to equilibrium again. This incremental erosion process continued until the pipe reached the critical pipe length of 19.7 cm, corresponding to a pipe position of $y = 0.158$ cm at a time of 4,920 s. At this point, the increase in the differential head triggered a transition to the progressive erosion phase in which the pipe progressed completely through the remainder of the sample without any further increase in the differential head.

The results of test B25-245 are summarized in Table 2. The sand sample had a relative density (D_r) of 0.577. The average hydraulic conductivity was determined to be $k = 3 \times 10^{-4}$m/s based on the measured flow rate and hydraulic gradient. This hydraulic gradient was calculated using a linear fit of the pressures measured by transducers P12 to P15 over the time period from 2,000 to 4,000 s. The hydraulic conductivity calculated in this manner was nearly constant for the entire time period as the pipe did not influence sensor P12 during this timeframe. As a result, the calculated value of the hydraulic conductivity was considered to be representative of the undisturbed sand in the entire sample.

This particular experiment was conducted to primarily study (1) the value of the critical head, H_c, or differential head that caused progressive erosion, and (2) to investigate the rate of erosion in the progressive phase[35]. The value of H_c that caused progressive erosion and failure was 5.4 cm which occurred when the erosion pipe was at the critical pipe length of $l_c = 19.7$ cm (corresponding to the pipe tip position of $y = 0.158$ m). However, as the focus of the present study is on evaluating FE models of

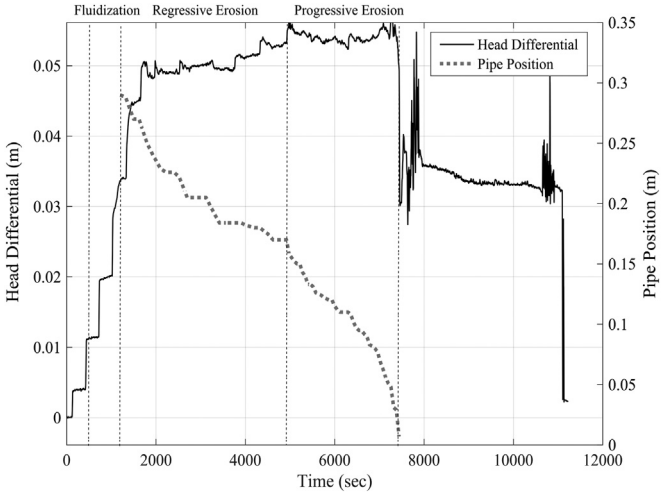

Fig. 6. Differential head (based on a projection of the 4 upstream [12–15] and 3 downstream [2–4] pressure transducers) and pipe y-position (distance from downstream end of the sample) for test B25-245.

the hydraulic solution with the pipe in equilibrium, the point of interest for this study is the equilibrium condition just prior to H_c being reached. At $t = 4,600$ seconds, the pipe was in equilibrium at the position of $y = 0.17$ m with an applied differential head of $H_{eq} = 0.052$ m.

A photograph of the pipe at y = 0.17 m is shown in Fig. 7. The pipe was estimated to be approximately 9 mm in width near the pipe tip and 5–6 mm in width along the erosion pipe. These visual estimates of the erosion pipe width were found to be slightly smaller than the dimensions determined through laser measurements. Unfortunately, no laser measurements of the pipe cross section were obtained when the pipe was in equilibrium at this location. A cross section was measured, however, at the y = 0.26 m transect when the pipe tip was located at y = 0.22 m (Fig. 8). From this cross section, we see that the pipe

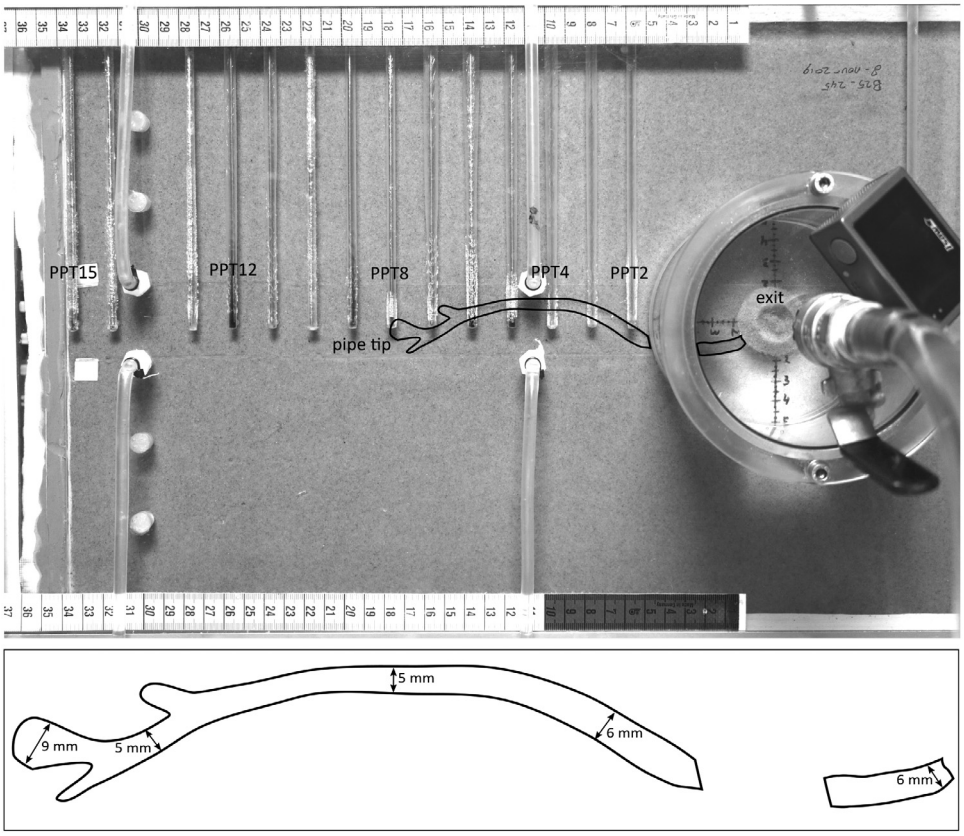

Fig. 7. Photograph of the experiment with the erosion pipe outlined when in equilibrium at y = 0.17 m. Visual estimates of the pipe widths were made based upon the photograph scale and visual edge of the pipe in the photograph.

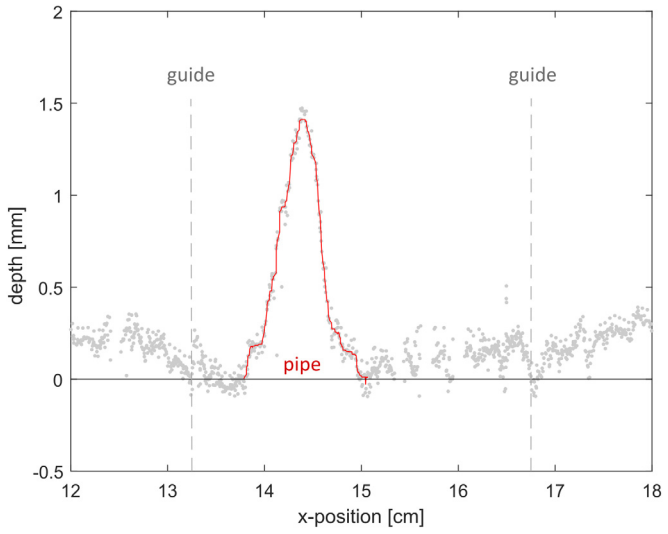

Fig. 8. Laser transect of the pipe cross section taken at y = 26 cm when the pipe tip was at y = 22 cm. Raw measurement indicated by gray dots and erosion pipe by red line. (For interpretation of the references to color in this figure legend, the reader is referred to the web version of this article.)

width is approximately 1 cm and the maximum pipe depth is approximately 1.5 mm. The pipe developed an additional 5 cm after this measurement was taken which causes increased flow rates through the pipe. As such, the dimensions of the actual erosion pipe when the tip is at y = 0.17 m are likely slightly larger than that shown in Fig. 8. The visually obtained measurements of pipe width in Fig. 7 are thought to be smaller than the laser width due to the fact that extremely shallow edges of the pipe may not be visible in the photograph. As such, the dimensions in Fig. 8 are thought to be the most reliable assessment of the actual pipe dimensions. The equilibrium position of the pipe shown in Fig. 7 will be modeled using the finite element model to evaluate how well the modeled solution compares to the head profile obtained from the pressure transducers.

4. Finite element analyses

Finite element models of test B25-245 were produced for the condition at t = 4,600 s with the pipe in equilibrium at y = 0.17 m. Models were developed for meshes of varying element sizes and pipe element types (line vs. hex). The following sections describe the various scenarios modeled and corresponding results.

Model description

The experiment was modeled as a symmetric half space as illustrated in Fig. 9. The half space was 0.1 m in height, 0.15 m in width, and 0.48 m in length. The downstream outlet hole was modeled as a 0.02 × 0.02 m square. In the half space model, the outlet dimensions correspond to a 0.01 m wide by 0.02 m long area with constant head boundary conditions set to $h = 0.0$ m. Representing the downstream exit area with a square that was larger than the actual 0.006 m diameter hole was found to be a suitable assumption and did not greatly impact the modeled heads. This is because (1) a void formed around the hole due to fluidization of the sand thereby creating an exit area larger than the hole alone and (2) the majority of the head loss was away from the exit hole due to the erosion pipe.

The erosion pipe was set to extend from the downstream exit area to a position 0.17 m from the upstream boundary. Models

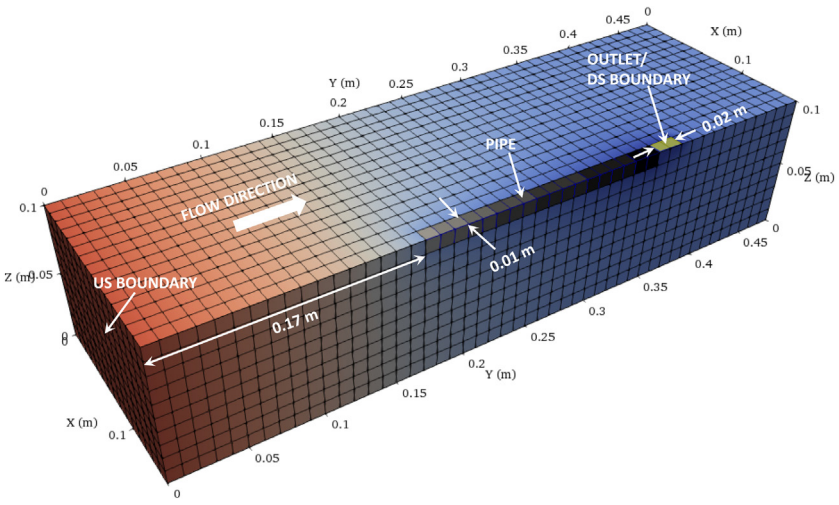

Fig. 9. Illustration of the symmetric half-space finite element mesh for representing the experiment. Example shown used 1 cm elements and hexahedral pipe elements.

Table 2
B25-245 test results.

Test number	D_r[-]	k [m/s]	Results			
			H_c [cm]	l_c [cm]	$i_{c,tip}$ [-]	H_{eq} *at y=0.17 m* [cm]
B25–245	0.577	3×10^{-4}	5.4	19.7	0.43	5.2

were run with the pipe represented by both hexahedral pipe elements (as shown in Fig. 9) and with 1D line elements to represent the pipe. When the pipe was represented by hexahedral elements, the width of the erosion pipe was determined by the total width of the elements used to represent the pipe. The pipe was fixed to a half space width of 0.01 m (0.02 m in total width) in all models using hexahedral elements to achieve precisely the same geometry with varied element sizes. Element sizes of 0.01 m, 0.005 m, and 0.002 m were used such that the pipe was represented using 1 element, 2 elements, and 5 elements to ensure the half space pipe width of 0.01 m remained constant when using hexahedral elements. In addition, one additional analysis with 0.005 m elements was run using a pipe width of 0.005 m (one element) to assess the influence of the pipe geometry on the results.

Models using 1D line elements for the pipes were also developed using mesh sizes of 0.01, 0.005, and 0.002 m elements. When using line elements, the width of the pipe was set to be a ratio of the pipe depth. A width (w) to depth (a) ratio of $w/a = 20$ was applied such that the cross-sectional area of the erosion pipe in the halfspace was given by

$$wa/2 = a \cdot \left(\frac{w}{a}\right) \cdot \frac{a}{2} = 10a^2.$$

The choice of $w/a = 20$ was made in an attempt to represent a similar pipe width as the 1 cm hexahedral representation for a pipe with an average depth of 1 mm (Fig. 8). That is, for a depth of 1 mm, a w/a ratio of 20 yields a pipe width of 20 mm which corresponds to a width of 10 mm, or 1 cm, in the halfspace model. In addition to making this assumption for line elements, an analysis was also conducted using line elements with the pipe width for the line elements fixed to 1 cm (regardless of pipe depth) to precisely match the scenario modeled with the hexahedral elements. Lastly, an analysis was also conducted with $w/a = 10$ to match the geometry of the actual pipe cross section shown in Fig. 8.

Table 3
Sand properties used in finite element models.

Test number	τ_c [Pa]	k [m/s]	d_{50} [mm]
B25–245	0.37	3.00E−04	0.228

The soil properties used in the models are provided in Table 3. The critical shear stress of the sand was determined by Pol et al.[35] to be 0.37 Pa. The hydraulic conductivity and grain size were measured as described previously.

To model the equilibrium conditions in test B25-245, the boundary conditions were set to the equilibrium boundary conditions in the experiment ($h = 0.052$ m upstream, $h = 0.00$ m downstream) with the pipe elements activated over the full critical pipe length as shown in Fig. 9. Iterations were conducted over the pipe depth in all pipe elements until the pipe depth was determined that satisfied the sediment equilibrium conditions. Once the pipe depth was determined, the coupled hydraulic solution was obtained which yielded the head distribution in the soil and the erosion pipe. The solutions obtained will be compared to the measured head values in the following section.

Results

The measured heads from the B25-245 experiment are compared to the modeled head distributions obtained from the finite element models in Fig. 10. A few observations can be made immediately from the results in Fig. 10. First, the results obtained using line elements with $w/a = 20$ to represent the erosion pipe are nearly all identical, regardless of the mesh size. Further, the results obtained using line elements tend to concentrate flow too severely near the upstream pipe tip which results in significant local head loss near the pipe tip and higher head values along the profile than measured. To the contrary, the simulations run with hexahedral pipe elements match the measurements much more closely, with the 1 cm and 5 mm elements giving the closest match to the measured values.

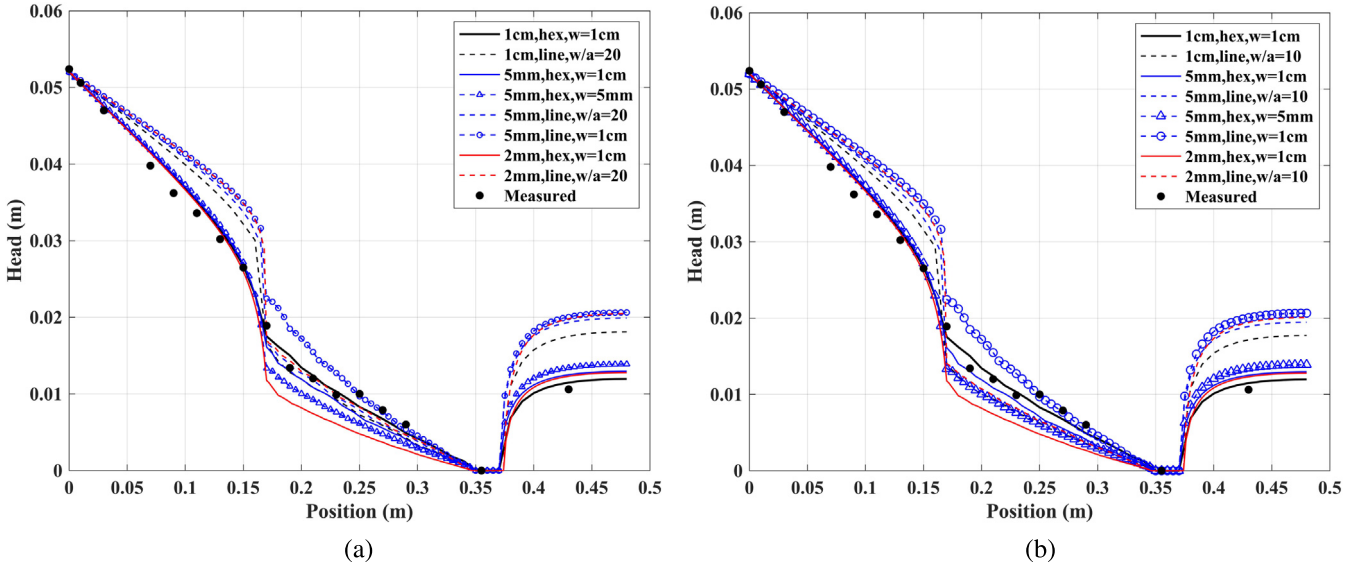

Fig. 10. Comparison of measured and modeled head distributions for t = 4,600 seconds with the pipe tip in equilibrium at y = 0.17 m for (a) w/a = 20 and (b) w/a = 10.

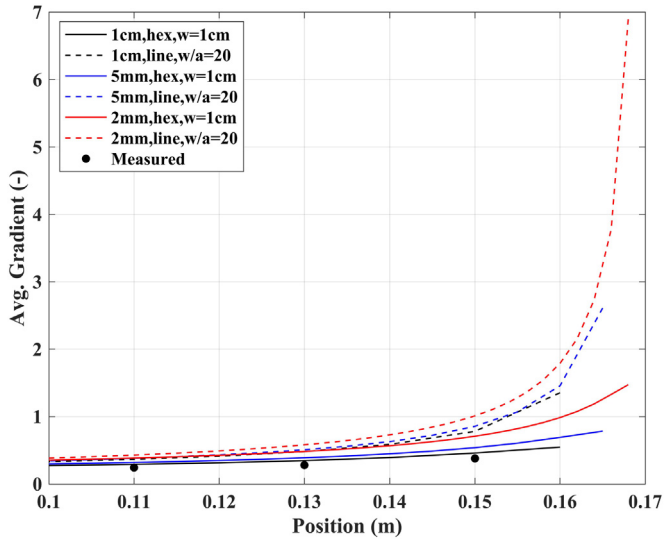

Fig. 11. Average hydraulic gradient at various positions in front of the pipe tip for FE solutions. (pipe tip is at the 0.17 m position).

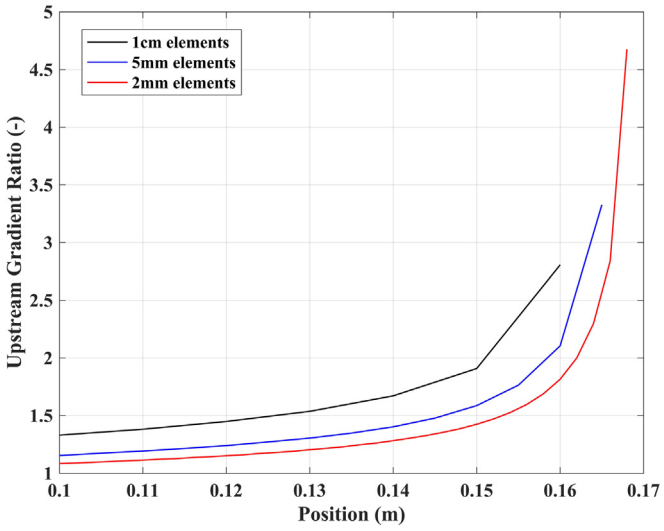

Fig. 12. Ratio of the hydraulic gradient calculated using linear pipe elements to the hydraulic gradient determined using hexahedral pipe elements for mesh sizes of 0.01 m.

With regards to the head profile in the erosion pipe, 3 of the measurements appear to match the slope of the hexahedral pipe element simulations and $w/a = 20$ line element simulations (sensors at positions of 0.19, 0.21, and 0.23), while 3 of the measurements appear to match the slope of the line element simulation with $w = 1$ cm (sensors at positions of 0.25, 0.27, and 0.29). By examining Fig. 7, it is seen that the pipe did not pass under the sensors at 0.25, 0.27, and 0.29 which may explain the slightly higher head values at these locations. The pipe is directly under the sensors at positions of 0.19, 0.21, and 0.23, however. As such, it appears that the pressure transducer measurements made in these positions are more representative of the actual head values in the erosion pipe. All simulations except for the analyses with 2 mm hexahedral elements, 5 mm hexahedral elements with $w = 5$ mm, and line elements of fixed width ($w = 1$ cm) accurately represented the head in the erosion pipe. The simulations using hexahedral elements of 0.002 m in size and $w = 5$ mm both underestimated the head profile in the pipe, whereas the simulation with $w = 1$ cm using line elements overestimated the head in the pipe. Potential reasons for this will be discussed in the following section.

The head profile upstream of the pipe tip was closely approximated by all of the FE analysis using hexahedral pipe elements. The head distribution and resulting hydraulic gradients and seepage velocities upstream of the pipe tip are of great interest as most numerical models evaluate pipe progression using these values[12,20,21,24,25,28,33,38]. As one can see from Fig. 10, the head profiles obtained using line elements are erroneously high. This is more clearly illustrated by examining the average hydraulic gradient over various distances in front of the erosion pipe. Fig. 11 shows the average hydraulic gradient between each position along the profile and the pipe tip at the 0.17 m position. Near the pipe tip location, the hydraulic gradients determined using the line element solutions are significantly higher than their counterparts determined using the hexahedral solutions. By calculating the ratio of the line to hex gradient (Fig. 12), we see that errors

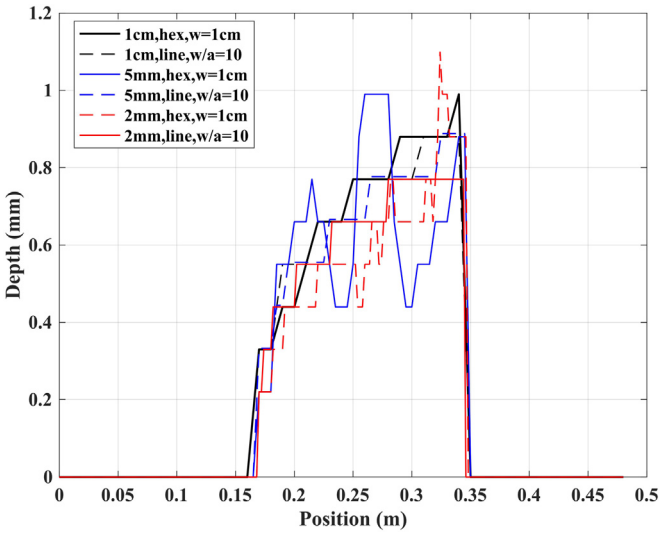

Fig. 13. Predicted depths of the erosion pipe obtained from the FE numerical solutions.

of 50%–300% would be obtained when using line elements if the same value of the critical, hydraulic gradient for pipe progression was used in both the hexahedral pipe element and linear pipe element simulations. This is a substantial error that may limit the usefulness of 1D linear elements for representing the erosion pipe. Potential explanations for the error in the linear pipe element solutions will be presented in Section 5 of this paper.

In addition to evaluating the head profiles and hydraulic gradients, it is also of interest to evaluate the predicted dimensions (namely pipe depth) obtained from the numerical solutions. Fig. 13 shows the calculated pipe depth profile along the centerline of the model (plane of symmetry in halfspace). The depth of the erosion pipe for the 1 cm, hexahedral pipe element solution approaches 1 mm near the end of the pipe. This is similar in magnitude to the actual depth of the erosion channel of 1.5 mm shown in Fig. 8. While the depth for the 1 cm hexahedral solution monotonically increases towards the maximum depth, the hexahedral solutions obtained with 5 mm and 2 mm elements vary along the pipe profile. This is due to the fact that the pipe does not maintain a constant pipe depth across the full pipe width (i.e., each pipe element has its own pipe depth). Fig. 14 shows the calculated depth of the erosion pipe in each pipe element for the 2 mm, hexahedral solution. Because the pipe is multiple elements wide, a "main channel" develops that has higher pipe depths than the remainder of the pipe. This narrower, deeper channel that develops results in higher hydraulic conductivities in the deep pipe elements (Eq. (13)) than if a more uniform, shallower channel were assumed. The higher pipe hydraulic conductivity explains why the 2 mm hexahedral solution yielded a lower head profile in the erosion pipe (Fig. 10). Further, the lower heads in the erosion pipe lead to the higher values of the calculated average gradient in front of the pipe (Fig. 11), despite the head profiles in front of the tip being nearly identical. From these observations, we see that the variable pipe depth provides an explanation for the apparent increase in average gradient with decreasing mesh size for simulations with hexahedral pipe elements.

5. Discussion

The analyses conducted using 1D line elements to represent the erosion pipe resulted in large errors in the solutions obtained. In general, errors in finite element solutions can be attributed to the following three sources[39]

1. *Quadrature and finite arithmetic errors* due to the numerical evaluation of integrals and numerical computation on a computer.
2. *Approximation error* due to the approximation of the solution using shape functions.
3. *Domain approximation error* due to the approximation of the problem domain by finite elements.

The first type of error, while present in all finite element solutions, is relatively small and cannot explain the 50%–300% error in the solutions obtained using line elements. The second type of error, approximation error, can be large in the vicinity of singularities where the solution is changing rapidly, especially when using linear basis functions. For elliptic PDE's with irregularities (as is the case for the present study), this type of error can be reduced by either increasing the refinement of the mesh in locations where the solution is changing rapidly or by increasing the order of the basis functions used in the finite element solution. As illustrated in Fig. 12, refining the mesh from 1 cm elements to 2 mm elements only increased the magnitude of the error in the solution obtained near the pipe tip. This suggests that the errors in the line element solutions are of the third type, domain approximation errors. While it seems intuitive that approximating the erosion pipe as a line would result in domain approximation errors, the magnitude of these errors was surprising as the erosion pipes are quite small (1 cm wide $\times$ 1 mm deep), and line elements were previously thought to be a suitable approximation. To further confirm that the errors are indeed due to domain approximation, the gradient in front of the pipe tip was compared for cases of w = 1 cm, w = 5 mm, and line elements (Fig. 15) to examine the influence of the pipe geometry on the upstream gradient. The results demonstrate that there is a smooth transition in the upstream gradient from the 1 cm wide, hexahedral geometry to the line element, further indicating that the errors are caused by the domain approximation error due to the poor physical representation of the pipe by the line elements. An explanation for the error can be provided by considering the number of elements connected to the pipe. For the case of line elements, only one soil element is connected to the pipe tip such that all of the flow into the pipe is conveyed through one element. This results in the high gradients. In the case of a single hexahedral element, the flow towards the pipe tip is spread across the four upstream elements connected to the hexahedral pipe element. As a result, the flow is spread out much more resulting in lower hydraulic gradients.

Without being addressed in some manner, the large domain approximation errors that result from using 1D pipe elements will lead to overly conservative solutions. As shown by the results obtained with 1 cm elements, the hydraulic gradients in front of the erosion pipe can be 50%–300% higher than the equivalent solution obtained using hexahedral pipe elements. Attempting to use the same physical criteria for erosion (whether based on gradient or velocity) in the two different discretizations will yield significantly differing differential heads at failure. This is unfortunate as 1D line elements are more convenient from a software development perspective and as a result have been more widely used (e.g., Refs. 25, 27). While additional research is needed to evaluate the issue further, this study has demonstrated that the errors can be significant and must be considered when performing numerical analysis of BEP. Non-standard numerical techniques may need to be explored in the future to accurately predict BEP progression. In particular, multi-scale modeling that makes use of coupled CFD-DEM simulations to simulate the pipe tip at the micro-scale may inherently capture the relevant processes for pipe progression. Alternatively, more advanced FEM techniques such as regularized solutions or enriched elements

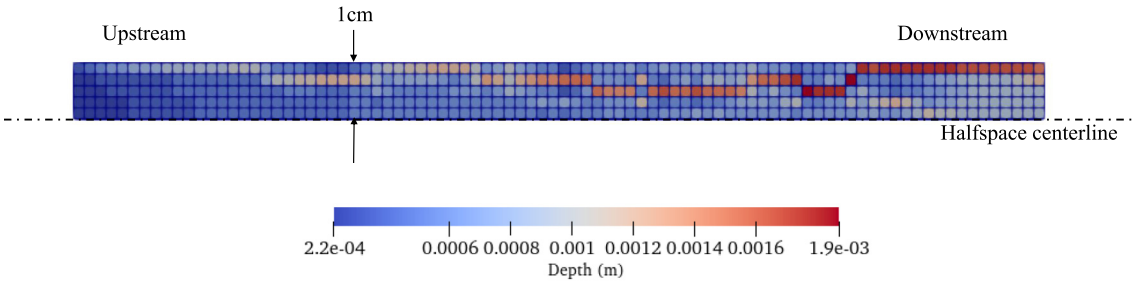

Fig. 14. Modeled depth of the erosion pipe for the 2mm hexahedral pipe element model (only the pipe domain is shown).

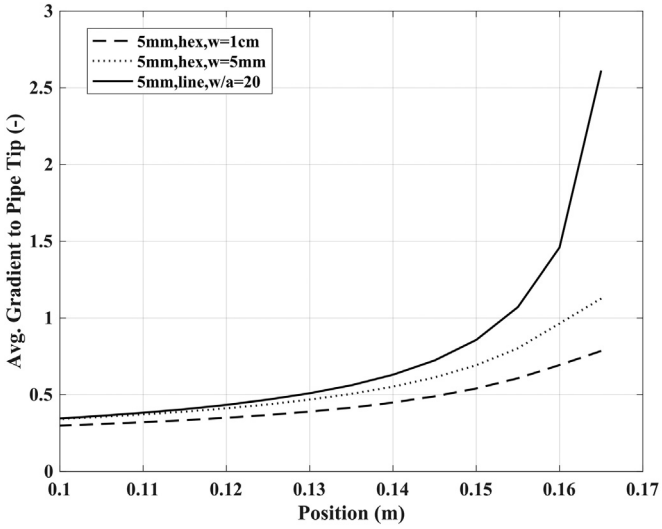

Fig. 15. Influence of the pipe geometry on the gradient upstream of the pipe.

(xFEM) may yield efficient approaches for accurately assessing BEP progression.

Lastly, an interesting observation can be made from the results presented regarding the geometry of the erosion pipe that yields the best hydraulic solution for the pipe gradients. From Fig. 10, it is seen that the line elements with $w/a = 20$ and the hexahedral elements with $w = 1$ cm yield the best fit to the experimental data. These simulations both correspond to a pipe width of approximately $w = 1$ cm in the halfspace because the pipe depth is approximately 1 mm. However, the actual pipe width (Fig. 8) was 1 cm in total suggests that the pipe width in the halfspace should have been only 5 mm. The model results with w = 5 mm and $w/a = 10$ should more closely represent the geometry of the actual experiment; however, both assumptions underpredicted the hydraulic gradient in the erosion pipe (Fig. 10). This suggests that the pipe width must be modeled as twice the actual pipe width to represent the hydraulic conditions in the pipe. One potential explanation for this discrepancy is the assumption that the pipe flow is simulated with equations for shallow rectangular ducts. Pipes with cross sectional shapes that are triangular, elliptical, or circular convey flow much more efficiently than parallel plates. As a result, the area of the modeled pipe channel must be larger than the actual pipe cross sectional area to represent the correct relationship between pressure gradient and flow.

6. Conclusions

Backward erosion piping (BEP) is a type of internal erosion responsible for the failure of many dams and levees worldwide. While many numerical models for predicting BEP have been proposed in the literature, an assessment of the error in the solutions these models provide has not been previously performed. This study evaluated the magnitude of errors in steady-state, finite element models of BEP progression via direct comparison of model results to measurements from a highly instrumented BEP experiment. Analyses were performed using both line elements and hexahedral elements to represent the erosion pipe with elements ranging in size from 0.002 m to 0.01 m. Results indicate that hexahedral elements provide a more accurate representation of the erosion pipe than one dimensional, linear elements yielding more accurate values of hydraulic gradient upstream of the pipe and overall head along the full model domain. However, using hexahedral elements requires realistic pipe dimensions (namely pipe width) to be represented in the mesh. Otherwise, the head profile in the erosion pipe will be underestimated.

On the other hand, the use of linear elements for the erosion pipe resulted in large domain approximation errors that caused 50%–300% errors in the computed values of the hydraulic gradient upstream of the pipe tip. Additionally, the linear pipe elements lead to artificially high heads along the full model domain. This is unfortunate as the solution obtained using line elements was not dependent on the mesh size as it was with hexahedral pipe elements. Additional research is necessary to develop approaches to account for these errors in BEP simulations when linear elements are used.

Lastly, for both hexahedral and line elements, it was found that the actual pipe width had to be modeled as twice the observed pipe width in the experiments to obtain a good fit. This is explained by the fact that the actual cross-sectional shape of the pipe is more closely described by a flat ellipse or triangle which convey flow more efficiently than a shallow rectangle of the same area. While other assumed channel shapes can be used, it appears from the results of this study that simply doubling the width of the pipe being represented yields an accurate solution.

CRediT authorship contribution statement

B.A. Robbins: Conceptualization, Methodology, Software, Formal analysis, Writing – original draft, Visualization. **V.M. van Beek:** Conceptualization, Methodology, Writing – review & editing. **J.C. Pol:** Investigation, Data curation, Writing – review & editing, Visualization. **D.V. Griffiths:** Software, Writing – review & editing.

Declaration of competing interest

The authors declare that they have no known competing financial interests or personal relationships that could have appeared to influence the work reported in this paper.

Acknowledgments

This paper was produced as part of an international cooperation between the USACE and Rijkswaterstaat, part of the Dutch Ministry of Infrastructure and the Environment. The authors express sincere gratitude to USACE and Rijkswaterstaat for this opportunity. The results are intended to inform the assessment and design of flood defenses.

References

1. Foster M, Fell R, Spannagle M. The statistics of embankment dam failures and accidents. *Can Geotech J*. 2000;37(10):1000–1024.
2. Richards KS, Reddy KR. Critical appraisal of piping phenomena in earth dams. *Bull Eng Geol Environ*. 2007;66(4):381–402. http://dx.doi.org/10.1007/s10064-007-0095-0.
3. Van Beek VM, Yao QL, Van MA. Backward erosion piping model verification using cases in China and the netherlands. In: *Seventh International Conference on Case Histories in Geotechnical Engineering*. Chicago, IL: 2013:1–7.
4. Robbins Bryant A, Van Beek VM. Backward erosion piping: A historical review and discussion of influential factors. In: *ASDSO Dam Safety*. New Orleans, LA: ASDSO; 2015:1–20.
5. Bligh WG. Dams, barrages and weirs on porous foundations. *Eng Rec*. 1910;64(26):708–710.
6. Clibborn J. *Experiments on the Passage of Water Through Sand*. Govt. of India, Central Printing Office; 1902.
7. De Wit JM. *Research Report on Sand Boil Model Tests*. Netherlands: Delft; 1984.
8. Hanses U, Müller-Kirchenbauer H, Savidis S. Zur Mechanik der rückschreitenden Erosion unter Deichen und Dämmen. *Bautechnik*. 1985;5:163–168.
9. Lane EW. Security from under-seepage masonry dams on earth foundations. *Trans ASCE*. 1935;100(1):1235–1272.
10. Pol JC, Kanning W, Jonkman SN. Temporal development of backward erosion piping in a large-scale experiment. *J Geotech Geoenviron Eng*. 2021;147(2):04020168. http://dx.doi.org/10.1061/(asce)gt.1943-5606.0002415.
11. Robbins BA, Montalvo-Bartolomei AM, Griffiths DV. Analyses of backward erosion progression rates from small-scale flume experiments. *J Geotech Geoenviron Eng*. 2020;146(9):04020093. http://dx.doi.org/10.1061/(asce)gt.1943-5606.0002338.
12. Robbins BA, Griffiths DV. Modelling of backward erosion piping in two- and three- dimensional domains. In: S. Bonelli & D Sterpi, ed. *Internal Erosion in Earth Dams, Dikes, and Levees, Vol. 17*. Cham, Switzerland: Springer Nature Switzerland AG; 2018:149–158. http://dx.doi.org/10.1007/978-3-319-99423-9.
13. Schmertmann JH. The no-filter factor of safety against piping through sands. In: Silva F, Kavazanijian EJ, eds. *Judgement and Innovation*. American Society of Civil Engineers.; 2000:65–133.
14. Townsend F, Schmertmann JH, Logan TJ, Pietrus TJ, Wong YW. *An Analytical and Experimental Investigation of a Quantitative Theory for Piping in Sand*. FLorida: Gainesville; 1981.
15. Van Beek Vera M, Robbins BA, Hoffmans GJCM, Bezuijen A, Van Rijn LC. Use of incipient motion data for backward erosion piping models. *Int J Sediment Res*. 2019;34(5):401–408. http://dx.doi.org/10.1016/j.ijsrc.2019.03.001.
16. Van Beek Vera M. *Backward Erosion Piping: Initiation and Progression*. Technische Universiteit Delft.; 2015. http://dx.doi.org/10.1007/s13398-014-0173-7.2.
17. Vandenboer K. *A Study on the Mechanisms of Backward Erosion Piping*. Ghent University; 2019.
18. Weijers J, Sellmeijer J. A new model to deal with the piping mechanism. *Filt Geotech Hydraulic Eng*. 1993;34:9–355.
19. Sellmeijer H, López J, Cruz D, Van Beek VM, Knoeff H. Fine-tuning of the backward erosion piping model through small-scale, medium-scale and ijkdijk experiments. *Eur J Environ and Civ Eng*. 2011;15(8):1139–1154. http://dx.doi.org/10.3166/EJECE.15.1139-1154.
20. Fascetti A, Oskay C. Dual random lattice modeling of backward erosion piping. *Comput Geotech*. 2019;105:265–276. http://dx.doi.org/10.1016/j.compgeo.2018.08.018.
21. Liang Y, Yeh T, Wang Y, Liu M, Wang J, Hao Y. Numerical simulation of backward erosion piping in heterogeneous fields. *Water Resour Res*. 2017;53:3246–3261. http://dx.doi.org/10.1002/2013WR014979, Reply.
22. Robbins BA, Griffiths DV. A two-dimensional, adaptive finite element approach for simulation of backward erosion piping. *Comput Geotech*. 2021;129:103820. http://dx.doi.org/10.1016/j.compgeo.2020.103820.
23. Robbins BA, Griffiths DV, Fenton GA. Influence of spatially variable soil permeability on backward erosion piping. In: *Proceedings of the 7th International Symposium on Geotechnical Safety and Risk*. 2019:96–101. http://dx.doi.org/10.3850/978-981-11-2725-0-bs2-cd.
24. Robbins Bryant A. Numerical modeling of backward erosion piping. *Proc 4th Itasca Symp Appl Num Model, (Itasca)*. 2016;55:1–558.
25. Rotunno AF, Callari C, Froiio F. A finite element method for localized erosion in porous media with applications to backward piping in levees. *Int J Numer Anal Methods Geomech*. 2019;43(1):293–316. http://dx.doi.org/10.1002/nag.2864.
26. Sellmeijer JB. Numerical computation of seepage erosion below dams (piping). In: *International Conference on Scour and Erosion*. 2006.
27. Van Esch JM, Sellmeijer JB, Stolle D. Modeling transient groundwater flow and piping under dikes and dams. In: *3rd International Symposium on Computational Geomechanics, Vol. 9*. 2013.
28. Wang D, Fu X, Jie Y, Dong W, Hu D. Simulation of pipe progression in a levee foundation with coupled seepage and pipe flow domains. *Soils Found*. 2014;54(5):974–984. http://dx.doi.org/10.1016/j.sandf.2014.09.003.
29. Zhou X, Jie Y, Li G. Numerical simulation of the developing course of piping. *Comput Geotech*. 2012;44:104–108. http://dx.doi.org/10.1016/j.compgeo.2012.03.010.
30. Lambe TW. Predictions in soil engineering. *Géotechnique*. 1973;23(2):151–202. http://dx.doi.org/10.1680/geot.1973.23.2.151.
31. Terzaghi K. Stability of slopes of natural clay. *Proc First Int Conf Soil Mech Found Eng*. 1936;1:161–165.
32. Skempton AW, Golder HQ. Practical examples of the $\phi = 0$ analysis of stability of clays. *Proc Second Int Conf Soil Mech Found Eng*. 1948;2:63–70.
33. Bersan S, Jommi C, Simonini P. Applicability of the fracture flow interface to the analysis of piping in granular material. In: *COMSOL Conference*. Rotterdam, Netherlands: 2013:1–8.
34. Smith IM, Griffiths DV. *Programming the Finite Element Method*. 4th ed Wiley; 2004.
35. Pol JC, Kanning W, Van Beek VM, Robbins BA, Jonkman SN. Temporal evolution of backward erosion piping in small-scale experiments. Manuscript submitted for publication.
36. Akrami S, Bezuijen A, Van Beek VM, Rosenbrand E, et al. Analysis of development and depth of backward erosion pipes in the presence of a coarse sand barrier. *Acta Geotech*. 2021;16:381–397. http://dx.doi.org/10.1007/s11440-020-01053-0.
37. Rosenbrand E, Van Beek V, Bezuijen A, Akrami S, Terwindt J, Koelewijn A, et al. Multi-scale experiments for a coarse sand barrier against backward erosion piping. *Géotechnique*. 2020:1–11. http://dx.doi.org/10.1680/jgeot.19.p.358, ahead of print.
38. Rahimi M, Shafieezadeh A. Coupled backward erosion piping and slope instability performance model for levees. *Transp Geotech*. 2020. http://dx.doi.org/10.1016/j.trgeo.2020.100394.
39. Junuthula Reddy. *An Introduction to the Finite Element Method*. United Kingdom: McGraw-Hill Education; 2006.